Eur. Phys. J. B **49**, 333–338 (2006)
DOI: 10.1140/epjb/e2006-00070-8

THE EUROPEAN PHYSICAL JOURNAL B

Transmission resonance via quantum bound states in confined arrays of antidots

Y.P. Chen[1], Y.E. Xie[1], and X.H. Yan[2,a]

[1] Institute of Modern Physics and Department of Physics, Xiangtan University, Xiangtan 411105, P.R. China
[2] College of Science, Nanjing University of Aeronautics and Astronautics, Nanjing 210016, P.R. China

Received 12 June 2005 / Received in final form 30 October 2005
Published online 10 March 2006

Abstract. We have studied the transmission resonances for a confined array of antidots, using the lattice Green's function method. Two kinds of resonant peaks via quasibound states are found. One kind of resonant peak corresponds to the split quasibound states. The split states originate from the superposition of quasibound states respectively localized in different (T or crossed) junctions, while the number of quasibound states in each junction is associated with the arm-width of the junction. Electrons in these split states are mainly localized in the junctions. The other kind of resonant peaks correspond to the high quasibound states which exist in (transverse and longitude) multi-period confined arrays of antidots. It is interesting to note that electrons in some of the high quasibound states are mainly localized in the intersection of the junctions rather than in the junctions themselves.

PACS. 73.22-f Electronic structure of nanoscale materials: clusters, nanoparticles, nanotubes, and nanocrystals – 73.20.-r Electron states at surfaces and interfaces

1 Introduction

Sophisticated modern growth technologies allow the construction of various mesoscopic structures [1] such as quantum wires and quantum dots, where carrier motion may be confined in at least one dimension. Because of the confinement effect, many interesting quantum phenomena are observed. One of them is the existence of quantum bound states in some classically unbound structures [2–10]. By calculating the energies and wave functions for an electron in crossed channels of infinite length, Schult et al. [2] have found quantum bound states in a crossed junction. Both experiment and theoretical calculations have indicated that in T-shaped [3] or L-shaped [4,5] channel(s) with infinite length, there can also exist one local bound state at the junction below the first transverse-mode energy. When the channels are sufficiently short, the quantum bound state localized in the junction couples to the continuous states and then becomes a quasibound state [6]. Thus, resonant tunneling via the quasibound state can occur [7]. This will bring about a resonant peak in conductance below the threshold of the first conductance plateau. For system which include more than one (crossed, T-shaped or L-shaped) junction, the interaction between the quasibound states localized in the different junctions is an interesting problem. Using the mode-matching technique, Wang et al. [8] studied the quantum bound states in a double-bend quantum channel of finite length connected to two two-dimensional (2D) electron gas reservoirs. It was found that there exists one resonant peak in conductance corresponding to one quasibound state for the quantum channel with double-bend continuity, and there exists two resonant peaks in conductance corresponding to two quasibound states for the quantum channel with double-bend discontinuity. The two quasibound states are symmetric and antisymmetric superpositions of two local bound states localized at two right-angle bends. Energies of these quasibound states are below the first conductance plateau. Ballistic transport in various nanostructures was studied by Ji and Berggren [9]. They showed that the bound states below the first sublevel split into several bound states due to the coupling of bound states in narrow ballistic channels with a few intersections. The number of split bound states is correlated with the number of intersections of the 2D semiconductor structure. Most of the former studies are focused on discussing the transmission resonance via the lowest energy quasibound state (ground state) localized in a relatively simple structure, however, high quasibound states will also induce transmission resonance [11] and many interesting transport properties are related to these states [12].

In this paper, we study transmission resonances via (ground and higher) quasibound states for a confined arrays of antidots (see Fig. 1), using the lattice Green's function method [13–16] We calculate conductance as a

[a] e-mail: xhyan@nuaa.edu.cn

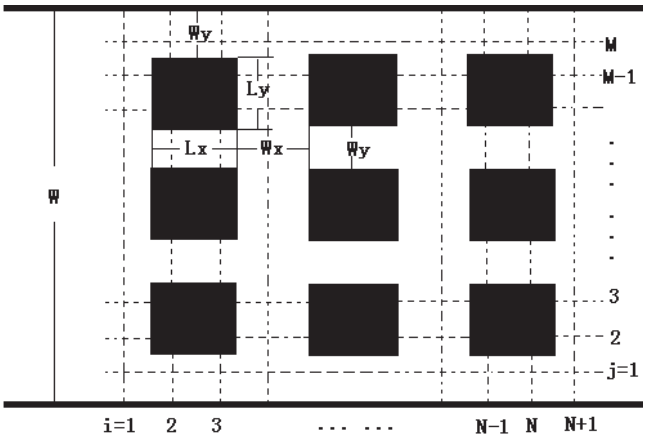

Fig. 1. Schematic view of the model, in which confined arrays of m(row)$\times n$(column) antidots are connected to the left and right leads. The squarelike antidots with electron potential P and dimensions L_x and L_y are placed with an equal transverse separation W_y and longitude separation W_x in a narrow constriction of width W.

function of electron energy for different geometries. The resonant peaks in conductance are associated with quasibound states which are shown by contour plots of probability density distribution. We discuss the influence of the separation between antidots arranged in lines on the quasibound states and the split states. The results indicate that the number of these states increases with the separation. The effects of the periodic increase of antidots in transverse and longitudinal directions on the high quasibound states are also discussed. Some interesting quasibound states in which electrons are localized in the intersection of the junctions rather than in the junctions have been found.

2 Model and method

Let us consider a finite-antidot array in a confined geometry which is connected to the left and right leads with width W (see Fig. 1). The antidots (black square area) have been modeled by squarelike potential barriers of size $L_x \times L_y$ and height P. The longitude and transverse separation between the antidots are W_x and W_y, respectively. Experiments on such systems have been carried out by Schuster et al. [17] In terms of a recursive Green's function (RGF) [13,14] scheme, one divides the system into a set of effective square lattices with lattice constant a. Hard wall boundaries are simply simulated by the absence of sites. To describe the electronic properties of the effective discretized system of a square lattice, one can define the tight-binding Hamiltonian [13]:

$$H = \sum_{i,j}(\varepsilon_{i,j}+P_{i,j})\,|i,j\rangle\,\langle i,j| + \sum_{i,j} V(|i,j\rangle\,\langle i,j+1| + \text{H.c.}) + \sum_{i,j} V(|i+1,j\rangle\,\langle i,j| + \text{H.c.}), \quad (1)$$

where $\varepsilon_{i,j}$ is the site energy and $P_{i,j}$ is additional potential at (i,j) site, and V are hopping matrix elements between the nearest neighboring sites respectively. Generally, $\varepsilon_{i,j} = -4V$ and $V = -\hbar^2/2m^*a^2$ ($m^* = 0.067m_0$ is the effective mass of an electron). We rewrite the Hamiltonian in units of column cell as

$$H = \sum_i H_i + \sum_i (H_{i,i+1} + H_{i+1,i}), \quad (2)$$

where H_i is the Hamiltonian of the ith isolated column cell, $H_{i,i+1}$ and $H_{i+1,i}$ are intercell Hamiltonian between the ith column cell and $(i+1)$th column cell with

$$H_{i+1,i} = \tilde{H}{}^*_{i,i+1}\,. \quad (3)$$

So the first two terms of equation (1) correspond to the first term of equation (2) and the last term of equation (1) corresponds to the second term of equation (2).

In terms of definition of Green's function $G = (E - H)^{-1}$, we construct the diagonal and off-diagonal Green's function by

$$\langle i|\,G^i\,|i\rangle = \langle i|\,(E - H^i)\,|i\rangle^{-1}, \quad (4)$$
$$\langle i|\,G^i\,|1\rangle = \langle i|\,(E - H^i)\,|1\rangle^{-1},$$

where E (in units of $-V$) is the electron energy, H^i is the total Hamiltonian for the strip comprising the 1th to ith column cells. In particular, $\langle 1|\,G^1\,|1\rangle$ of the 1th column cell and $\langle N+1|\,G^{N+1}\,|N+1\rangle$ of $(N+1)$th column cell represent Green's functions of the left and right leads respectively. So $\langle N+1|\,G\,|1\rangle$ represents the systematic Green's function which couples those from the 1th to the $(N+1)$th column cell. According to the Dyson equation $G = G^0 + G^0\,\hat{V}\,G$, a set of recursive formulas can be obtained [14]

$$\langle i+1|\,G^{i+1}\,|i+1\rangle^{-1} = E - H_{i+1} - H_{i+1,i}\,\langle i|\,G^i\,|i\rangle\,H_{i,i+1}, \quad (5)$$

$$\langle i+1|\,G^{i+1}\,|1\rangle = \langle i+1|\,G^{i+1}\,|i+1\rangle\,H_{i+1,i}\,\langle i|\,G^i\,|1\rangle. \quad (6)$$

We start recursion from $\langle 1|\,G^1\,|1\rangle$. According to equation (5), the following sequences of Green's functions: $\langle 1|\,G^1\,|1\rangle \to \langle 2|\,G^2\,|2\rangle \to \cdots \to \langle N|\,G^N\,|N\rangle$ can be generated. Substituting these Green's functions into equation (6), we can obtain $\langle 2|\,G^1\,|1\rangle \to \langle 3|\,G^2\,|1\rangle \to \cdots \to \langle N|\,G^N\,|1\rangle$ in turn. In the final recursion step we attach the right lead, and then obtain the Green's function $\langle N+1|\,G\,|1\rangle$.

The Green's function $\langle N+1|\,G\,|1\rangle$ allows us to calculate the transmission coefficient T of the two-terminal system [13,14]. Then conductance G is represented by Landauer-Buttiker formula

$$G = \frac{2e^2}{h}T. \quad (7)$$

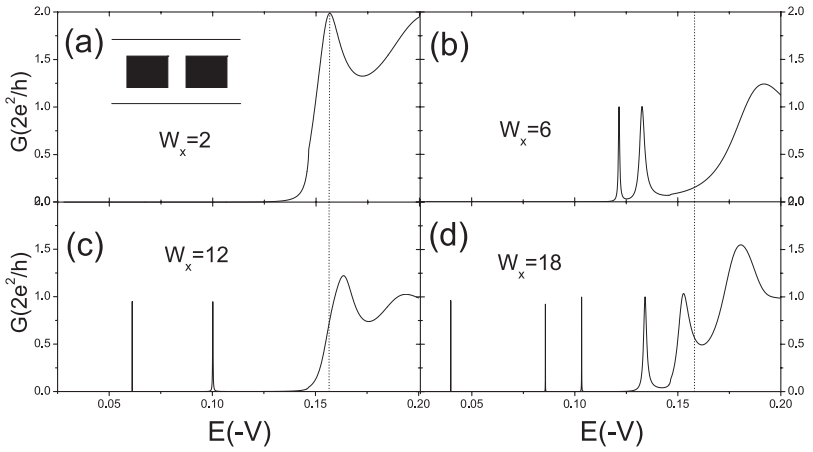

Fig. 2. Calculated conductance as a function of electron energy for the simplest array in the insert of (a), which includes two antidots with separation W_x. (a) $W_x = 2$, (b) $W_x = 6$, (c) $W_x = 12$, (d) $W_x = 18$. Other parameter of the structure is $L_x = 10, L_y = 10, W_y = 6$ and $P = 50$. The dotted line represents the first threshold energy $E_1 = \hbar^2\pi^2/2m^*W_y^2$. (The length is in units of lattice constant a and the energy is in units of $-V$.)

To calculate the eigen-energy E of the structure and corresponding wave function Ψ, we write the Hamiltonian of the system as

$$H = H_0 + \Sigma, \tag{8}$$

where H_0 is the total Hamiltonian of the antidot array associated with equation (1), Σ is the total self-energies of the two leads [14]. Solving the eigen-equation $H\Psi = E\Psi$, one can obtain the eigen-energy E and wave function Ψ. In general, the eigenvalue is complex, whose imaginary part is associated with the lifetime of the eigenstate.

3 Results and discussion

We first consider an element array including two longitude antidots, as shown in the insert of Figure 2a. There are two T junctions in the middle region of the structure. In Figure 2, the calculated conductance for the simplest confined array with different longitude separation W_x of antidots are presented. For narrower separation, only one high resonant peak with value 2 ($2e^2/h$) appears in conductance just below the first threshold energy E_1 ($E_1 = \hbar^2\pi^2/2m^*W_y^2$) (see Fig. 2a). As the separation is increased to $W_x = W_y$, Figure 2b shows that there are two peaks with value 1 ($2e^2/h$) in conductance. Comparing with the peak in Figure 2a, the two peaks shift to low energy. With wider separation, more resonant peaks appear in the conductance below the threshold energy, as shown in Figures 2c and 2d, and the first two peaks further shift to lower energy with an enlarged distance between them. The results can be explained by the character of the quasibound states localized in the confined array. It is well known that, as the arm of a (crossed or T) junction changes from infinite length to finite length, the bound state localized in the junction will develop into a quasibound state. This will induce resonant tunneling via the quasibound state. When the separation between antidots is narrower, only one quasibound state exists in each T junction and the wave function of the state hardly penetrates to the lateral arm (the intersection of the two T junctions). So the two quasibound states respectively localized at the upper and below T junctions are independent, i.e., without interaction. In this case, the two states have the same energy while the resonant peaks induced by them superpose into a high peak in the conductance profile. As the separation W_x becomes wide, the wave functions of the two quasibound states can deeply extend into the lateral arm. Then interaction between the two states occurs. Due to the symmetric and antisymmetric superposition of the two wave functions, two-fold split states with different energies are formed in the confined array. We respectively depict in Figures 3a and 3b the contour plots of probability density of the two split states. The

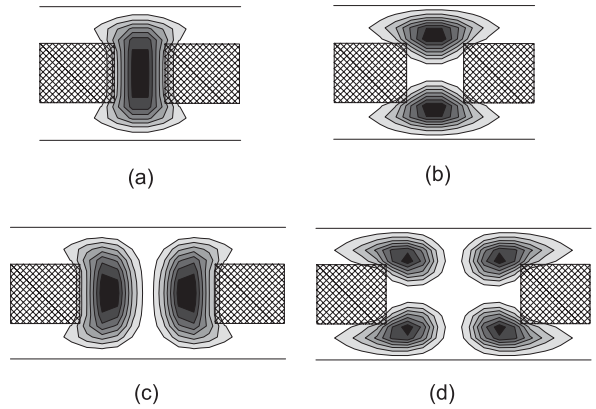

Fig. 3. Contour plots of probability density distribution of the quasibound state (a) corresponding to the first resonant peak with $E = 0.1217$ in Figure 2b, (b) corresponding to the second resonant peak with $E = 0.1327$ in Figure 2b, (c) corresponding to the third resonant peak with $E = 0.1032$ in Figure 2d, (d) corresponding to the fourth resonant peak with $E = 0.1343$ in Figure 2d. The innermost contour curve possesses the highest probability density and the shaded areas represent antidots.

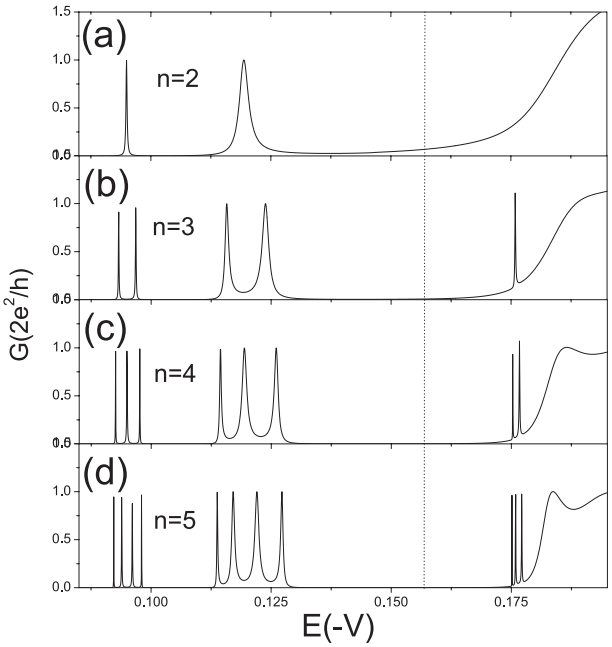

Fig. 4. Calculated conductance as a function of electron energy for confined arrays including n longitude antidots with $W_x = 8$. (a) $n = 2$, (b) $n = 3$, (c) $n = 4$, (d) $n = 5$. Other parameters of the structure are $L_x = 10, L_y = 10, W_y = 6$ and $P = 50$. The dotted line represents the first threshold energy $E_1 = \hbar^2\pi^2/2m^*W_y^2$. (The length is in units of lattice constant a and the energy is in units of $-V$.)

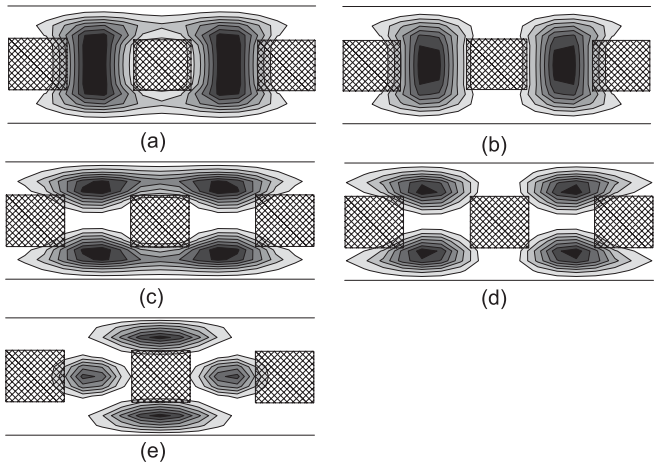

Fig. 5. Contour plots of probability density distribution of the quasibound states corresponding to the five resonant peaks in Figure 4b (a) corresponding to the first resonant peak with $E = 0.0932$, (b) corresponding to the second resonant peak with $E = 0.0967$, (c) corresponding to the third resonant peak with $E = 0.1159$, (d) corresponding to the fourth resonant peak with $E = 0.124$, (e) corresponding to the fifth resonant peak with $E = 0.1760$. The innermost contour curve possesses the highest probability density and the shaded areas represent antidots.

energy difference of the two states is proportional to the strength of interaction between the states, while the average energy is equal to the energy of quasibound states in a single junction [8]. Corresponding to the two states, two resonant peaks appear in Figure 2b. In addition, the energy of a quasibound state in a single T junction decreases with the increase of the lateral-arm width [18]. So the wider separation leads to the two peaks in Figure 2b shifting to low energy. As one continues to increase the separation W_x, on one hand, it increases the energy difference of the two split bound states since the distance of the first two peaks in conductance is wider, on the other hand, high quasibound states will exist in each T junction except the ground state. The interaction of the high quasibound states forms high split states. In Figure 2d, the third and the fourth peaks correspond to two high split states, which are induced by the interaction of the second lowest quasibound state localized in each junction. Figures 3c and 3d display the contour plots of probability density of the two higher quasibound states corresponding to the third and fourth resonant peak in Figure 2d, respectively. One can see that the two states are odd-parity states whose wave functions are taken to be odd symmetry to the center line of the T junction, while the two states in Figure 3a and 3b are even-parity states. As a result, increasing the wider separation W_x causes more resonant peaks via higher split states emerging in the conductance profiles, and the position of peaks shift to low energy.

In Figure 4, we show the conductance as a function of electron energy for the confined array including n periodic antidots in a longitudinal direction. As $W_x = 8$, only a quasibound state is localized in each T-junction. So, when $n = 2$, there are two resonant peaks via the split states appearing in conductance below the threshold energy (Fig. 4a). When the confined array consists of three longitude antidots ($n = 3$), the structure has four T junctions. In each two transverse T junctions, there exist two split states. Due to the longitude symmetric and antisymmetric superposition of the split states, each split state localized in two transverse T junctions further splits into two new split states. Accordingly, each peak in Figure 4a splits into two peaks in Figure 4b. In Figures 5a–5d the contour plots of probability density of the four new split states corresponding to the first four resonant peaks in Figure 4b are displayed. It is clearly seen that the new split states displayed in Figures 5a and 5b are formed by symmetric and antisymmetric superposition of two states depicted in Figure 3a, while the states displayed in Figures 5c and 5d are formed by symmetric and antisymmetric superposition of the two states depicted in Figure 3b. Electrons in these split states are mainly localized at the junctions. In addition, in the high energy region a resonant peak appears at the edge of the first conductance plateau in Figure 4b. This resonant peak is induced by a high quasibound state which contour plot of probability density is displayed in Figure 5e. It is interested to see that the electrons in this state are not localized at the T junctions but at the intersections of T junctions. When the structure includes more antidots, more split states localized in each two transverse T junctions are added to the structure. The interaction of the split states lead to each split state in the case $n = 2$ splitting into $n-1$ states. So there are $2(n-1)$ peaks via $2(n-1)$ split states in the

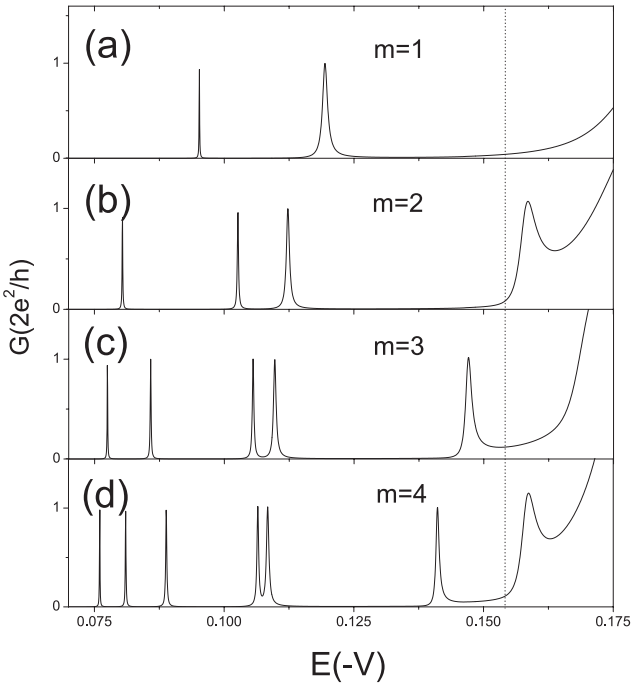

Fig. 6. Calculated conductance as a function of electron energy for confined arrays including $m(row)\times 2(column)$ antidots with $W_x = 8$. (a) $m = 1$, (b) $m = 2$,(c) $m = 3$,(d)$m = 4$. Other parameters of the structure are $L_x = 10, L_y = 10, W_y = 6$ and $P = 50$. The dotted line represents the first threshold energy $E_1 = \hbar^2\pi^2/2m^*W_y^2$. (The length is in units of lattice constant a and the energy is in units of $-V$.)

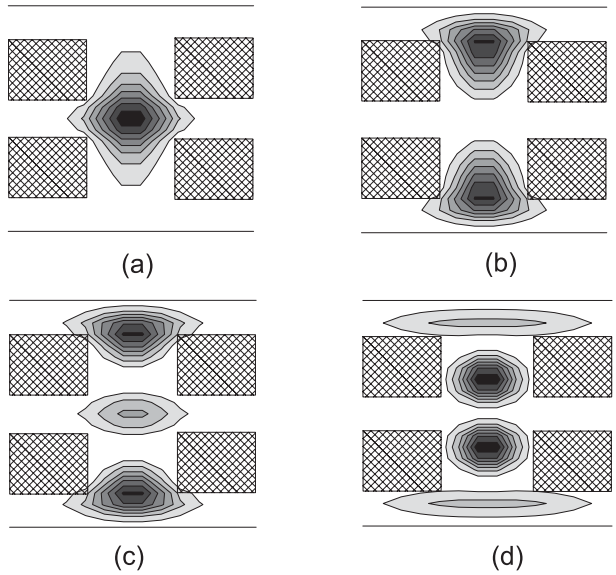

Fig. 7. Contour plots of probability density distribution of the quasibound states corresponding to the four resonant peaks in Figue 6b. (a) corresponding to the first resonant peak with $E = 0.0802$, (b) corresponding to the second resonant peak with $E = 0.1027$, (c) corresponding to the third resonant peak with $E = 0.1123$, (d) corresponding to the fourth resonant peak with $E = 0.1584$. The innermost contour curve possesses the highest probability density and the shaded areas represent antidots.

conductance below the first threshold energy (see Figs. 4c and 4d). While $n-2$ resonant peaks via higher quasibound states appear at the edge of the first conductance plateau. It can be expected that, as n is large, the conductance for the finite periodic array will form a miniband and minigap structure, and the resonant peaks are related to the miniband.

The influence of the periodic increase of antidots in the transverse direction on the resonant peaks is then considered. In Figure 6, we present the conductance for the confined array including $m(row) \times 2(column)$ antidots. As the array consists of two rows of antidots ($m = 2$), there are two T junctions and one crossed junction in the structure. It is seen that the conductance profile in Figure 6b exhibits three resonant peaks below the threshold energy. The peaks are induced by the three quasibound states localized in the three junctions. The energy of the quasibound state in a crossed junction is lower than that in a T junction, as the crossed and T junctions have the same-width arms. So the first peak corresponds to the quasibound state localized in the crossed junction, while the latter two peaks are induced by two split states localized in the T junctions. Figures 7a–7c display respectively the contour plots of probability density distribution of the three states. The existence of the crossed junction weakens the interaction of the upper and lower T-shaped quasibound states, thus, comparing with the two peaks in Figure 6a, the second and the third resonant peaks in Figure 6b become closer. In addition, in the higher energy region, we can find a resonant peak via a high quasibond state whose contour plots of probability density is depicted in Figure 7d. From Figures 7a to 7d, the wave functions are in turn taken to be even- and odd-symmetry about the parallel center line of the crossed junctions, which is due to symmetric potential distribution and the hard walls of up and lower boundaries. The electrons in the former three quasibound states are mainly localized in the junctions while electrons in the fourth quasibound states are mainly localized at the intersections of these junctions. So the fourth state belongs to the whole structure rather than any single junction. As the confined array includes m row antidots, there are $m-1$ crossed junctions in the structure. Due to the interaction of local states in the $m-1$ crossed junctions, $m-1$ split states are formed and thus the first resonant peak in Figure 6b splits into $m-1$ peaks (see Figs. 6c and 6d). At the same time, more crossed junctions further weaken the interaction of the local states in the two T junctions, leading to the two resonant peaks via the T split states becoming closer. Moreover, with the transverse increase of the space between two column antidots, the energy of the high quasibound states decreases and more higher quasibound states will exist in the structure. This results in more resonant peaks appearing around the first threshold energy.

In Figure 8, we depict the conductance as a function of electron energy for the confined array including multi-row ($m = 3$) and multi-column n antidots. It is found that the resonant peaks in conductance can be divided into three groups. The first group located at the lowest

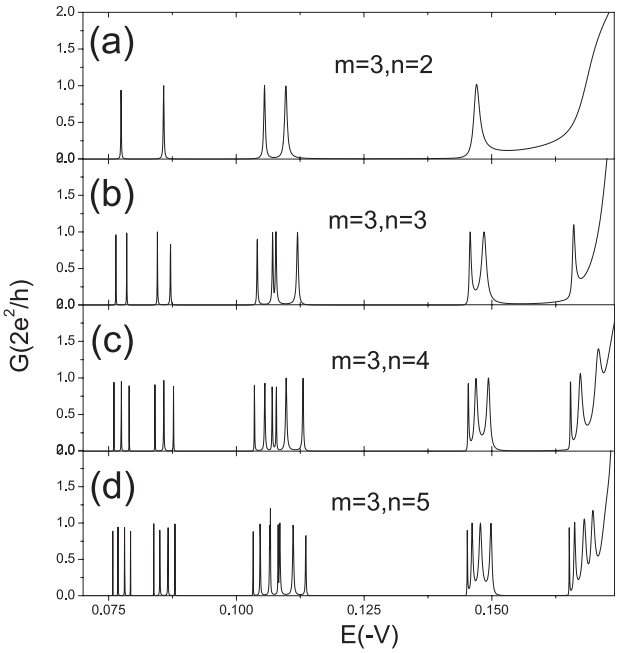

Fig. 8. Calculated conductance as a function of electron energy for confined arrays including $3(row) \times n(colum)$ antidots with $W_x = 8$. (a) $n = 2$, (b) $n = 3$, (c) $n = 4$, (d) $n = 5$. Other parameters of the structure are $L_x = 10, L_y = 10, W_y = 6$ and $P = 50$. (The length is in units of lattice constant a and the energy is in units of $-V$.)

energy range has $(m-1) \times (n-1)$ peaks corresponding to $(m-1) \times (n-1)$ split quasibound states mainly localized in the $(m-1) \times (n-1)$ crossed junctions. The second-group peaks are mainly induced by the interaction of the $2(n-1)$ local T-shaped quasibound states, and the number of peaks will be equal to $2(n-1)$, i.e., the number of T junctions. The third group of peaks appear at around the first threshold energy. These peaks correspond to the high quasibound states which are induced by transverse and longitude periodic increase of antidots. Electrons in these states have high probabilities of being localized at the intersection of junctions.

4 Conclusions

By using the lattice Green's function method, we have studied the resonant peaks via the quasibound states for a confined array of antidots. Split quasibound states will be formed through symmetric and antisymmetric superposition of quasibound states in different junctions, while the number of quasibound states in a single junction is related to the separation of longitude antidots. As the confined array consists of n (crossed and T) junctions and each junction only has one quasibound state, n resonant peaks via the n split states appear in the conductance below the first threshold energy. Electrons in these split states are mainly localized in the junctions. In the high energy region (around the first threshold energy), some resonant peaks via higher quasibound states are also found. The number of the higher quasibound states is associated with the periodic number of antidots and geometry. Electrons in the some of these quasibound states are not localized at the junctions but at the intersections of the junctions.

This work was supported by Major Project of State Ministry of China (Grant No. 204099) and the Project Supported by Scientific Research Fund of Hunan Provincial Education Department (No. 02C572).

References

1. Supriyo Datta, *Electronic Transport in Mesoscopic systems* (Cambridge University Press, 1997)
2. R.L. Schult, D.G. RavenHall, H.W. Wyld, Phys. Rev. B **39**, 5476 (1989)
3. A.R. Goñi, L.N. Pfeiffer, K.W. West, A. Pinczuk, H.U. Baranger, H.L. Stormer, Appl. Phys. Lett. **61**, 1956 (1992); L.A. Openov, Europhys. Lett. **55**, 539 (2001)
4. F. Sols, M. Macucci, Phys. Rev. B **41**, 11887 (1990); Y.K. Lin, Y.N. Chen, D.S. Chuu, Phys. Rev. B **64**, 193316 (2001); J. Appl. Phys. **91**, 3054 (2002)
5. J. Goldstone, R.L. Jaffe, Phys. Rev. B **45**, 14100 (1992)
6. K.-F. Berggren, Z.-L. Ji, Phys. Rev. B **43**, 4360 (1991)
7. P.J. Price, Phy. Rev. B **48**, 17301 (1993); Semicond. Sci. Technol. **9**, 899 (1994)
8. Chuan-Kui Wang, K.F. Berggren, Zhen-Li Ji, J. Appl. Phys. **77**, 2564 (1995)
9. Zhen-Li Ji, Karl-Fredrik Berggren, Phys. Rev. B **45**, 6652 (1992)
10. Y. Avishai, D. Bessis, B.G. Giraud, G. Mantica, Phys. Rev. B **44**, 8028 (1991)
11. Zhi-an Shao, Wolfgang Porod, Craig S. Lent, Phys. Rev. B **49**, 7453 (1994)
12. Yuan Ping Chen, Xiao Hong Yan, Yue E. Xie, Phys. Rev. B **71**, 245335 (2005)
13. F. Sols, M. Macucci, U. Ravaioli, K. Hess, Appl. Phys. Lett. **54**, 350 (1989); F. Sols, M. Macucci, U. Ravaioli, K. Hess, J. Appl. Phys. **66**, 3892 (1989)
14. T. Ando, Phys. Rev. B **44**, 8017 (1991)
15. D. Guan, U. Ravaioli, R.W. Giannetta, M. Hannan, I. Adesida, M.R. Melloch, Phys. Rev. B **67**, 205328 (2003)
16. M.J. McLennan, Yong Lee, Supriyo Datta, Phys. Rev. B **43**, 13846 (1991)
17. R. Schuster, K. Ensslin, D. Wharam, S. Kühn, J.P. Konhaus, G. Böhm, W. Klein, G. Tränkle, G. Weimann, Phys. Rev. B **49**, 8510 (1994)
18. Y.K. Lin, Y.N. Chen, D.S. Chuu, Phys. Rev. B **64**, 193316 (2001)